

Obtuse triangle suppression in anisotropic meshes[☆]

Feng Sun^{a,*}, Yi-King Choi^a, Wenping Wang^a, Dong-Ming Yan^{a,b,c}, Yang Liu^{b,d}, Bruno Lévy^b

^a Department of Computer Science, The University of Hong Kong, Pokfulam Road, Hong Kong, China

^b LORIA/INRIA Lorraine, Project ALICE, Campus scientifique 615, rue du Jardin Botanique, 54600, Villers les Nancy, France

^c Geometric Modeling and Scientific Visualization Center, KAUST, Thuwal 23955-6900, Saudi Arabia

^d Microsoft Research Asia, 5/F, Beijing Sigma Center, No. 49, Zhichun Road, Haidian District, Beijing, 100190, China

ARTICLE INFO

Article history:

Received 6 August 2010

Received in revised form 3 August 2011

Accepted 28 September 2011

Available online 4 October 2011

Keywords:

Triangulation

Minkowski metric

Anisotropic mesh

Surface remeshing

Obtuse triangles

ABSTRACT

Anisotropic triangle meshes are used for efficient approximation of surfaces and flow data in finite element analysis, and in these applications it is desirable to have as few obtuse triangles as possible to reduce the discretization error. We present a variational approach to suppressing obtuse triangles in anisotropic meshes. Specifically, we introduce a *hexagonal Minkowski metric*, which is sensitive to triangle orientation, to give a new formulation of the centroidal Voronoi tessellation (CVT) method. Furthermore, we prove several relevant properties of the CVT method with the newly introduced metric. Experiments show that our algorithm produces anisotropic meshes with much fewer obtuse triangles than using existing methods while maintaining mesh anisotropy.

© 2011 Elsevier B.V. All rights reserved.

1. Introduction

Anisotropic meshes are used to approximate surfaces or flow fields for rendering and simulation (Cohen-Steiner et al., 2004; Dey et al., 2007; Valette et al., 2008). For anisotropic triangle meshes to be used in finite element methods (FEM), it has been well established (Babuska and Aziz, 1976; Bern and Eppstein, 1992a; Shewchuk, 2002) that the accuracy and convergence of the interpolation function in FEM are greatly influenced by the maximal angle of a triangle element. Triangles with large angles are also found to hamper the efficiency of some iterative algebraic solvers (Du et al., 2005). This implies that obtuse triangles should be avoided as much as possible.¹ The control of the maximum angle is difficult, however. Existing methods for anisotropic triangulation always produce meshes that contain a large number of obtuse triangles.

There are a number of methods for computing anisotropic triangulations. The algorithms in Leibon and Letscher (2000), Cheng et al. (2006), Labelle and Shewchuk (2003) compute an anisotropic Voronoi diagram of some fixed data points, whose dual is an anisotropic triangulation. To allow unconstrained vertices, a number of methods have been proposed (e.g., Bossen and Heckbert, 1996; Shimada, 1997; Du et al., 2005; Wang and Du, 2005; Jiao et al., 2006; Boissonnat et al., 2008). Anisotropic triangulations that minimize interpolation errors of an underlying function or surface are characterized in Simpson (1994), Rippl (1992). Based on similar considerations, data-dependent triangulation of fixed data points is studied in Dyn et al. (1990, 2001). However, none of these methods consider avoiding obtuse triangles.

[☆] This paper has been recommended for acceptance by Kai Hormann.

* Corresponding author.

E-mail addresses: fsun@cs.hku.hk (F. Sun), ykchoi@cs.hku.hk (Y.-K. Choi), wenping@cs.hku.hk (W. Wang), dmyan@cs.hku.hk (D.-M. Yan), liuyang@loria.fr (Y. Liu), levy@inria.fr (B. Lévy).

¹ In some cases where the mesh anisotropy is dictated by the anisotropy of a PDE to be solved on the mesh, obtuse triangles with certain orientations are acceptable (Shewchuk, 2002).

While nonobtuse triangulation has been the topic of considerable research, little is known about how to remove or suppress obtuse triangles in anisotropic triangulations. Existing methods for computing nonobtuse triangulations (e.g., Baker et al., 1988; Bern and Eppstein, 1992b; Li and Zhang, 2006; Brandts et al., 2009) are not applicable to anisotropic meshes as they do not take the anisotropy requirement into consideration. In this paper, we present an effective method for suppressing obtuse triangles in anisotropic triangle meshes while maintaining mesh anisotropy. Our contribution is the introduction of a novel *hexagonal Minkowski metric* in the formulation of the centroidal Voronoi tessellation (CVT) method, based on which a variational method is devised for computing anisotropic meshes. In addition, we also prove several properties of the CVT method with the newly introduced metric. Our method is capable of producing anisotropic triangulations that have much fewer obtuse triangles than using existing methods.

2. Preliminaries

A commonly used approach to anisotropic triangulation is based on *anisotropic centroidal Voronoi tessellation* (anisotropic CVT). In this approach, an energy function is first defined for a set of points, called *seeds*, in a compact domain Ω . This energy function is then minimized to determine the optimal distribution of the seeds. Finally, a triangle mesh is obtained by taking the seeds as mesh vertices and using the dual of the Voronoi diagram of the seeds to determine edge connectivity of the mesh. Two keys to successful application of such a CVT-based method are: 1) the formulation of an appropriate CVT energy function reflecting the desired mesh quality criteria (e.g., anisotropy, orientation control, mesh density); and 2) the development of effective optimization schemes for minimizing this function (e.g., initialization, convergence, avoidance of poor local minima).

We will briefly introduce the concepts of *anisotropic CVT*, on which our triangulation algorithm is based. We first present the basics about isotropic centroidal Voronoi tessellation (isotropic CVT) which are necessary for a good understanding of anisotropic CVT. We assume a two-dimensional compact domain Ω for the simplicity of explanation, but the concepts to be introduced apply also to the more general domains, including surfaces.

2.1. Isotropic CVT

Let $\mathbf{X} = (\mathbf{x}_i)_{i=1}^n$ be an ordered set of points, called *seeds* or *generators*, in Ω . The Voronoi cell Ω_i , also called the CVT cell, of a seed \mathbf{x}_i is

$$\Omega_i = \{ \mathbf{x} \in \Omega \mid d(\mathbf{x}, \mathbf{x}_i) \leq d(\mathbf{x}, \mathbf{x}_j), \forall j \neq i, j = 1, 2, \dots, n \}$$

where $d(\mathbf{x}, \mathbf{y})$ is the Euclidean distance between the points \mathbf{x} and \mathbf{y} . The collection of the Voronoi cells Ω_i of all the seeds \mathbf{x}_i constitutes a Voronoi tessellation (or Voronoi diagram) of Ω . A *constrained centroid* of Ω_i is the point in Ω_i that is closest to the centroid (i.e., the centre of mass) of Ω_i ; note that the constrained centroid agrees with the centroid when the centroid is inside Ω_i . A *centroidal Voronoi tessellation*, or CVT, is a special Voronoi tessellation in which each seed \mathbf{x}_i coincides with the constrained centroid \mathbf{c}_i of its Voronoi cell Ω_i (Du et al., 1999).

From a variational standpoint, a CVT is characterized by a critical point (i.e., a gradient-vanishing point) of the following isotropic CVT energy function (Du et al., 1999)

$$F(\mathbf{X}) = \sum_{i=1}^n F_i(\mathbf{X}) = \sum_{i=1}^n \int_{\Omega_i} d^2(\mathbf{x}, \mathbf{x}_i) d\sigma \quad (1)$$

where $d\sigma$ is the differential area element of Ω . In practice, we seek to compute a CVT corresponding to a local minimizer of $F(\mathbf{X})$ and such a CVT will be called a *stable CVT*. Furthermore, a CVT given by a global minimizer of $F(\mathbf{X})$ will be called an *optimal CVT*. The most commonly used method for minimizing the CVT energy function is the Lloyd's method (Du et al., 1999), and a more efficient quasi-Newton method is recently proposed by Liu et al. (2009).

According to the celebrated Gershó's conjecture (Gershó, 1979), as the number of seeds increases, the Voronoi cells $\{\Omega_i\}$ of an optimal CVT generated by the isotropic CVT energy function $F(\mathbf{X})$ in Eq. (1) are asymptotically congruent regular hexagons. Gershó's conjecture has been proved in two dimensions by Gruber (1999) and supported by strong evidences in three dimensions (Du and Wang, 2005). Consequently, for an optimal CVT, the energy values $F_i(\mathbf{X})$ of all the CVT cells in Eq. (1) are asymptotically equal. Taking the dual of such a hexagonal mesh yields an isotropic triangle mesh with nearly equilateral triangle faces.

2.2. Anisotropic CVT

An anisotropic triangulation is computed with the CVT framework using a Riemannian metric in place of the Euclidean metric in the CVT energy function.

A Riemannian metric tensor M is defined by a positive definite quadratic form $Q(\mathbf{p}; \mathbf{v}) = \mathbf{v}^T \mathbf{M}(\mathbf{p}) \mathbf{v} : \mathcal{T}_{\mathbf{p}} \rightarrow \mathbb{R}$ in the two-dimensional tangent space $\mathcal{T}_{\mathbf{p}}$ of each point $\mathbf{p} \in \Omega$, where $\mathbf{v} \in \mathcal{T}_{\mathbf{p}}$. Since the metric M in $F_E(\mathbf{X})$ has an elliptic form, the iso-distance curves under this metric are ellipses centred at \mathbf{p} . The figure below shows the so-called *unit ellipse* $\mathcal{E} : \bar{\mathbf{v}}^T \mathbf{M}(\mathbf{p}) \bar{\mathbf{v}} = 1$

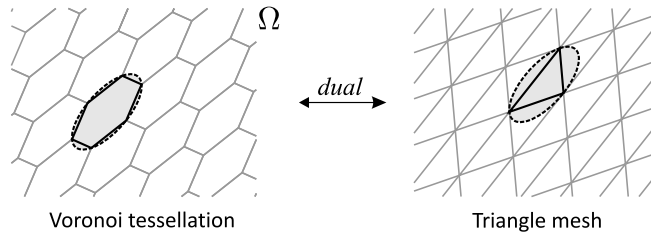
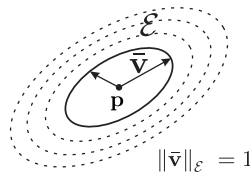


Fig. 1. An anisotropic CVT and its dual triangulation.

(in solid line), on the tangent plane of a point \mathbf{p} , with the dashed lines being iso-distance curves which are called the *metric ellipses*. Equipped with the metric M , the domain Ω becomes a two-dimensional Riemannian manifold. Then the anisotropic CVT energy function is

$$F_E(\mathbf{X}) = \sum_{i=1}^n \int_{\Omega_i} d_E^2(\mathbf{x}, \mathbf{x}_i) d\sigma \tag{2}$$

where $d_E(\mathbf{x}, \mathbf{y})$ is the geodesic distance between the points \mathbf{x} and \mathbf{y} on Ω with respect to the metric M , and Ω_i is the Voronoi cell of the seed \mathbf{x}_i defined with respect to M . A CVT computed by minimizing $F_E(\mathbf{X})$ is an *anisotropic CVT*, since its Voronoi cells are elongated along the direction dictated by the metric M . To distinguish it from another type of anisotropic CVT we are going to introduce, we will call it the *elliptic CVT*. Similarly, we may define the stable elliptic CVT and the optimal elliptic CVT, corresponding to the local and global minimizers of $F_E(\mathbf{X})$, respectively. Taking the dual of an elliptic CVT yields an anisotropic triangulation (see Fig. 1).



The shape of the Voronoi cells in an elliptic CVT can be deduced via the correspondence between an elliptic CVT of a two-dimensional Riemannian manifold Ω and an isotropic CVT of a two-dimensional manifold $\hat{\Omega}$ in some higher-dimensional Euclidean space, which is established by Nash’s embedding theorem (Nash, 1956). According to this correspondence (see Appendix A for details), within the corresponding tangent planes of Ω and $\hat{\Omega}$, a Voronoi cell of the elliptic CVT of a seed point $\mathbf{p} \in \Omega$ is locally the image under an affine mapping of a regular hexagonal Voronoi cell of the isotropic CVT of $\hat{\Omega}$. The linear part of this affine mapping is given by a matrix \mathbf{G} such that $\mathbf{G}^T \mathbf{G} = \mathbf{M}^{-1}(\mathbf{p})$, where $\mathbf{M}(\mathbf{p})$ is the metric at \mathbf{p} . Hence, each Voronoi cell of an elliptic CVT of a seed \mathbf{p} is asymptotically an *affinely regular hexagon* (i.e., a regular hexagon under an affine mapping) inscribed to some metric ellipse \mathcal{E}' at \mathbf{p} . Furthermore, the triangles in the dual anisotropic triangulation of an elliptic CVT have the same anisotropy defined by \mathcal{E}' (see Fig. 1).

Note that the factorization $\mathbf{G}^T \mathbf{G} = \mathbf{M}^{-1}(\mathbf{p})$ above is not unique, since there is also $(\mathbf{Q}\mathbf{G})^T (\mathbf{Q}\mathbf{G}) = \mathbf{M}^{-1}(\mathbf{p})$ for any orthogonal matrix \mathbf{Q} . It means that any affinely regular hexagonal regions H of different orientations inscribed to a metric ellipse at \mathbf{p} in Ω corresponds to a regular hexagon (of different orientations) inscribed to the same metric circle in $\hat{\Omega}$. Since the embedding of Ω as $\hat{\Omega}$ preserves the CVT energy of each Voronoi cell, all H ’s of different orientations thus have the same elliptic CVT energy (Fig. 2(a)). The elliptic CVT energy function $F_E(\mathbf{X})$ is therefore oblivious to the orientation of the Voronoi cells in an elliptic CVT and minimizing $F_E(\mathbf{X})$ does not have any control over the orientations of the anisotropic CVT cells that it generates.

The orientation of a Voronoi cell in an anisotropic CVT, however, can greatly affect the shape of the dual triangle. Fig. 3 shows two sets of hexagonal cells with different orientations inscribed to some metric ellipse of the same anisotropy. It can be seen that while the cells in Fig. 3(a) generate obtuse triangles in the dual mesh, those in Fig. 3(b) yield acute triangles. Consequently, the lack of orientation control in an elliptic CVT generally leads to the larger number of obtuse triangles in the resulting anisotropic triangulation.

3. Hexagonal Minkowski metric

To enable the control of orientations of CVT cells, we introduce the *hexagonal Minkowski metric* in the CVT energy function. This metric is a special case of the Minkowski metric, also known as convex metric (Valentine, 1964). It can represent the same mesh anisotropy as the Riemannian metric and is sensitive to CVT cell orientations.

Given an ellipse \mathcal{E} in \mathbb{E}^2 centred at the origin \mathbf{o} , let H be an affinely regular hexagon inscribed in \mathcal{E} (see the figure below). The hexagon H defines a vector norm, denoted by $\|\mathbf{v}\|_H$, for vectors $\mathbf{v} \in \mathbb{R}^2$ — H is the “unit disk” in the sense that

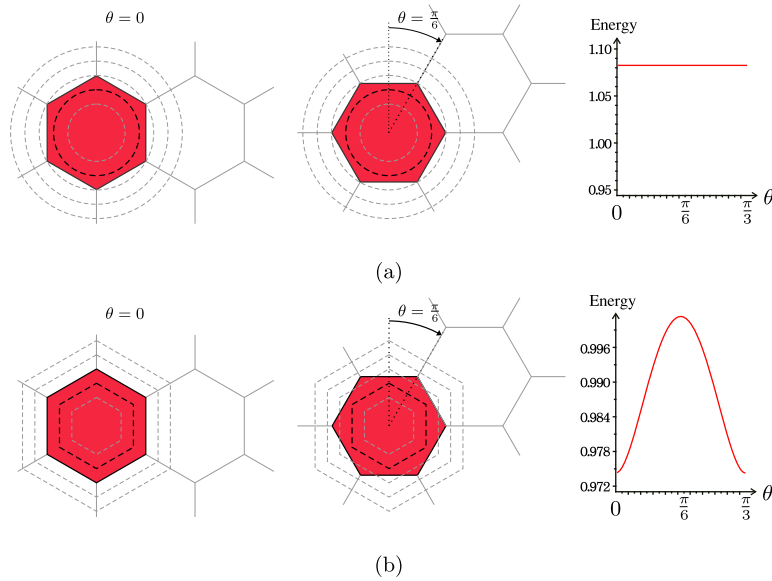
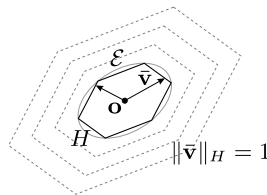


Fig. 2. (a) The elliptic CVT energy remains constant for hexagonal cells with different orientations. (b) The HM CVT energy varies with the orientation of the hexagonal CVT cell. The dashed lines in black and in grey are the unit ellipse and metric ellipses in (a), and the unit hexagon and metric hexagons in (b), respectively.

$\|\bar{\mathbf{v}}\|_H = 1$ for any vector $\bar{\mathbf{v}}$ on H , and $\|k\mathbf{v}\|_H = |k| \cdot \|\mathbf{v}\|_H, \forall k \in \mathbb{R}$ and $\forall \mathbf{v} \in \mathbb{E}^2$; hence, H is called a *unit hexagon*. The norm $\|\mathbf{v}\|_H$ will be called the *hexagonal Minkowski metric* or *HM metric* for short. For any two points \mathbf{x} and \mathbf{y} in \mathbb{E}^2 , their distance induced by the HM metric is $d_H(\mathbf{x}, \mathbf{y}) = \|\mathbf{x} - \mathbf{y}\|_H$, and is called the *HM distance*. All the points \mathbf{y} having the same HM distance to \mathbf{x} lie on the same *metric hexagon* that is a uniformly scaled image of H centred at \mathbf{x} (the dashed hexagons in the figure below).



The CVT energy function based on the HM metric, called the *HM CVT energy*, is defined as

$$F_H(\mathbf{X}) = \sum_{i=1}^n F_{H,i}(\mathbf{X}) = \sum_{i=1}^n \int_{\Omega_i} d_H^2(\mathbf{x}, \mathbf{x}_i) d\sigma. \tag{3}$$

The CVT computed by minimizing $F_H(\mathbf{X})$ will be called the HM CVT, which is a new kind of anisotropic CVT. Fig. 2(b) shows that the CVT energy $F_{H,i}(\mathbf{X}) \equiv \int_{\Omega_i} d_H^2(\mathbf{x}, \mathbf{x}_i) d\sigma$ of a hexagonal cell Ω_i (in red) has different values when the CVT cell assumes different orientations. The energy reaches its minimum when the CVT cell has the same orientation as H . This suggests that we may control the orientation of CVT cells by minimizing the energy function $F_H(\mathbf{X})$ defined with an appropriate HM metric.

Let $\bar{F}_{\mathbf{c}}(s) = \int_{U(s, \mathbf{c})} d_H^2(\mathbf{x}, \mathbf{c}) d\sigma$ denote the CVT energy of a seed \mathbf{c} with a Voronoi cell $U(s, \mathbf{c})$ which is a uniformly scaled image of H centred at a point \mathbf{c} and has area s . It is shown in Sun et al. (2010) that $\bar{F}_{\mathbf{c}}(s)$ is indeed the minimum CVT energy among all regions of area s and that $\bar{F}_{\mathbf{c}}(s)$ is convex. Therefore, $F_H(\mathbf{X})$ has a lower bound $m\bar{F}_{\mathbf{c}}(\frac{|\Omega|}{m})$ when m , the number of seeds, is fixed. Moreover, when m approaches infinity, the affect due to the boundary of the domain Ω becomes negligible. The following theorem depicts the CVT pattern induced by the HM metric when the CVT energy $F_H(\mathbf{X})$ approaches its lower bound.

Theorem 1. Let Ω be a convex compact region in \mathbb{E}^2 and (\mathbf{X}_m) be a finite set of points in \mathbb{E}^2 with $|\mathbf{X}_m| = m$, for $m = 1, 2, \dots$, such that

$$F_H(\mathbf{X}_m) \sim m\bar{F}_{\mathbf{c}}\left(\frac{|\Omega|}{m}\right) \text{ as } m \rightarrow \infty,$$

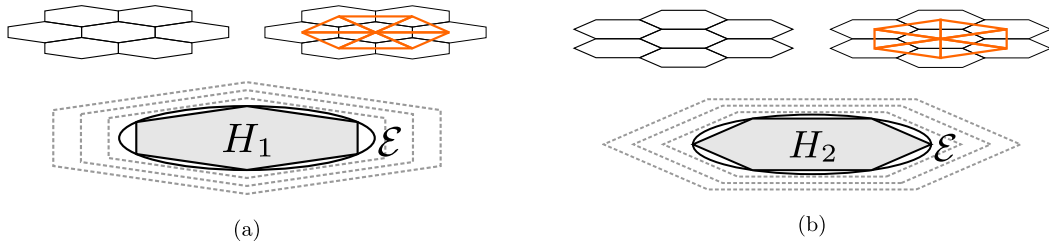


Fig. 3. (a) The CVT and its dual triangulation generated by the unit hexagon H_1 . (b) The CVT and its dual triangulation generated by the unit hexagon H_2 . It can be seen that the resulting triangle mesh contains obtuse triangles in (a) and contains acute triangles in (b).

where H represents a regular hexagonal Minkowski metric. Then \mathbf{X}_m is asymptotically a regular hexagonal pattern of edge length $(\frac{2|\Omega|}{3\sqrt{3}m})^{1/2}$, in which the hexagons are with the same orientation as H .

The proof is given in Sun et al. (2010). In fact, it can also be shown that when H is an affinely regular hexagon, \mathbf{X}_m asymptotically assumes a hexagonal pattern in which each hexagon has the same shape and orientation as H . The anisotropy of H is therefore inherited in the hexagonal pattern and its dual triangle mesh.

We now consider choosing a unit hexagon to avoid obtuse triangles. Suppose that a part of a planar domain is endowed uniformly with HM metrics specified by the two unit hexagons H_1 and H_2 of different orientations as shown in Fig. 3, respectively. As H_1 and H_2 are inscribed by the same metric ellipse, they define the same mesh anisotropy. It can be seen that the triangulation corresponding to H_1 consists of obtuse triangles (Fig. 3(a)), while the triangulation corresponding to H_2 consists of acute triangles only (Fig. 3(b)). Therefore in order to suppress obtuse triangles, we opt to use the unit hexagon H_2 in Fig. 3(b), which is characterized by having one of its diagonals aligned with the major axis of the metric ellipse.

In general, the Riemannian metric \mathbf{M} is inconstant and varies over the domain. The shape of the optimal triangle mesh that maintains the anisotropy of the domain with minimal number of obtuse triangles is therefore unknown in theory. In this case, we may define an H_2 metric that adapts with \mathbf{M} . When the metric \mathbf{M} varies smoothly, it can be considered as locally approximately constant, and it is expected that the H_2 metric should lead to a triangle mesh which maintains anisotropy locally and at the same time suppresses obtuse triangles. Our experimental results in Section 5 indeed demonstrate that the triangle mesh thus obtained with the H_2 metric not only maintains the varying anisotropy well, but also contains much fewer obtuse triangles, as compared with that using the elliptic metric \mathbf{M} .

4. Algorithm

We assume the input is a domain Ω endowed with an HM metric tensor H , with proper orientations as shown in Fig. 3(b) to suppress obtuse triangles. Our algorithm comprises the following steps:

Main algorithm

- Step 1:** Initialization—Randomly distribute a set of n initial seeds $\mathbf{X} = \{\mathbf{x}_i\}$ on Ω .
 - Step 2:** Perform an HM CVT optimization.
 - Step 3:** Perform k passes of the following refinement step (or until a specific target reduction in the number of obtuse triangles is met):
 - 3.1) Carry out an elliptic CVT optimization to cluster obtuse triangles.
 - 3.2) Randomly perturb the seeds which are incident to obtuse triangles.
 - 3.3) Carry out an HM CVT optimization to suppress obtuse triangles.
 - Step 4:** Return the dual triangle mesh of the final optimized Voronoi tessellation as the resulting mesh.
-

Step 3 of the main algorithm serves to help the optimization to escape from a poor local minimum through perturbation, and hence to further reduce the number of obtuse triangles. Our tests show that a typical number of k is 10 which works well for a moderate number of seeds. This refinement step will be explained in detail in subsequent subsections.

Both the HM CVT and the elliptic CVT optimizations in the main algorithm are computed using the same framework as follows:

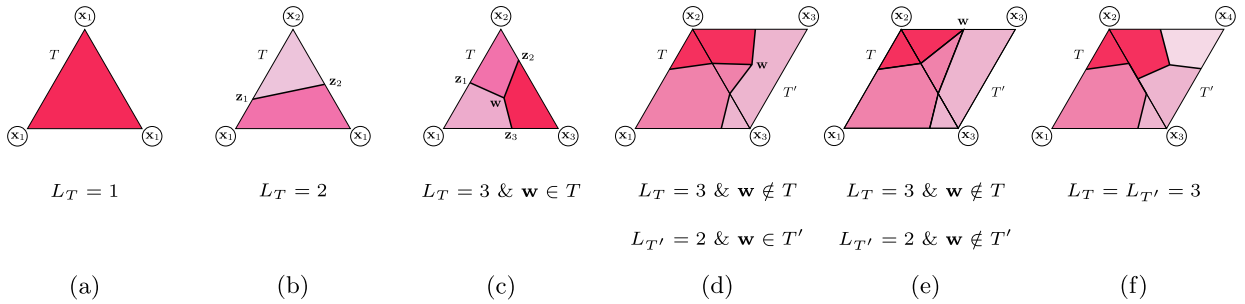


Fig. 4. Computing the Voronoi cell boundaries in an input mesh triangle T . Each triangle vertex is labelled with its closest seed and L_T is the number of different labels at the vertices of T . (a) $L_T = 1$ and no boundary should lie in T . (b) $L_T = 2$ and the Voronoi cell boundary is a line connecting the bisection points on the edges of T . (c) $L_T = 3$ and a Voronoi cell vertex \mathbf{w} is found in T . (d) If $\mathbf{w} \notin T$, we locate \mathbf{w} on a neighbouring triangle T' with $L_{T'} = 2$. (e) Further if $\mathbf{w} \notin T'$, the tracking stops and \mathbf{w} is snapped to an edge of T' . (f) The tracking also stops if $L_{T'} = 3$.

CVT optimization framework

Perform m iterations of the following optimization steps:

- Step 1:** Compute the Voronoi cells of \mathbf{X} , the energy terms $F_i(\mathbf{X})$ and the gradient $\nabla F_i(\mathbf{X})$ of each seed \mathbf{x}_i .
- Step 2:** Use the L-BFGS algorithm, an effective quasi-Newton method, to obtain a new set of seeds \mathbf{X}' . Project \mathbf{X}' to Ω . Replace \mathbf{X} by \mathbf{X}' .
-

In the above CVT framework, the difference between computing an elliptic CVT and computing an HM CVT is that they use different ways of computing the Voronoi cells, the energy terms and the gradient terms, according to their respective metrics. This framework differs from the conventional CVT optimization framework in that instead of looping through until convergence of $F_i(\mathbf{X})$, we perform only a specific number of iterations (m) for the optimization steps out of efficiency consideration. The termination of the optimization is determined by the number of refinement steps taken in the main algorithm. Our implementation uses $m = 50$ iterations for all CVT optimizations which has demonstrated a satisfactory performance in our framework.

In the following we will present some implementation details of our method.

4.1. Computing Voronoi diagram

The existence of Delaunay triangulations on Riemannian manifolds has been established in Leibon and Letscher (2000), assuming sufficiently dense seeds. An anisotropic Voronoi diagram on a Riemannian manifold is so defined that the distance between points is given by the length of the shortest geodesics with respect to a Riemannian metric. To facilitate computation, this distance is usually approximated so that the bisectors between two seeds can be simplified as conic sections or quadric surfaces (Jiao et al., 2006). Different methods for computing anisotropic Voronoi diagrams have been presented in Cheng et al. (2006), Labelle and Shewchuk (2003), Boissonnat et al. (2008). However, no practical implementations of these methods are known that work for mesh surfaces.

Our method computes a discrete approximation of anisotropic Voronoi diagrams on a triangulation of the input domain Ω . The number of triangle elements of the input mesh needs to be high enough, as compared with the size of the output mesh, to ensure sufficient accuracy. A ratio of about 10 : 1 is generally recommended. We also adopt the convention in Du and Wang (2005) in which the metric tensor is defined at the input mesh vertices.

To determine the Voronoi tessellation given seeds \mathbf{X} on Ω , we compute an approximation to the Voronoi cell boundaries, each of which is the bisector of two seeds $\mathbf{x}_1, \mathbf{x}_2 \in \mathbf{X}$. A point $\mathbf{x} \in \Omega$ on the bisector has equal distances to \mathbf{x}_1 and \mathbf{x}_2 , that is, $d_H(\mathbf{x}, \mathbf{x}_1) = d_H(\mathbf{x}, \mathbf{x}_2)$. Vertex-flooding as in Cohen-Steiner et al. (2004) is first used to label each vertex in Ω with its nearest seed point with respect to H . Our idea is to process each triangle T to locate any bisector that it may intersect.

For each triangle T , we locate the bisection points \mathbf{z}_i on the sides of T whose endpoints have different labels using the bisection method (Fig. 4). If the vertices of T are of three different labels, we first determine a bisecting line l equidistant to two seeds \mathbf{x}_1 and \mathbf{x}_2 , and attempt to locate a Voronoi vertex \mathbf{w} in T equidistant to all three seeds on l . If \mathbf{w} is not in T , we shall seek its location in a neighbouring triangle T' (Fig. 4(d)–(f)). Out of computational efficiency consideration, these treatments are not exhaustive and only serve to approximate the Voronoi boundaries.

4.2. Iterative solver

We use the limited memory BFGS method, also called the *L-BFGS method* (Liu and Nocedal, 1989), to minimize the CVT energy function $F_H(\mathbf{X})$. The L-BFGS method is a variant of the classical BFGS, which is an iterative quasi-Newton method. The L-BFGS method takes as an input a set of seeds \mathbf{X} , the CVT energy $F_H(\mathbf{X})$ and its gradient $\nabla F_H(\mathbf{X})$, and returns the new positions for \mathbf{X} . To compute the CVT energy $F_{H,i}(\mathbf{X})$ of each Voronoi cell Ω_i , we use a triangulation \mathcal{T}_i of Ω_i from the preceding computation of the Voronoi diagram. Let Δ_j be a triangle in \mathcal{T}_i . The energy term $F_{H,i}(\mathbf{X})$ is approximated as:

$$F_{H,i}(\mathbf{X}) = \sum_{\Delta_j \in \mathcal{T}_i} \int_{\Delta_j} d_H^2(\mathbf{x}, \mathbf{x}_i) d\sigma \approx \sum_{\Delta_j \in \mathcal{T}_i} f(\Delta_j)$$

where $f(\Delta_j)$ is the approximate CVT energy contributed by the triangle Δ_j , given by the quadrature (Hillion, 1977)

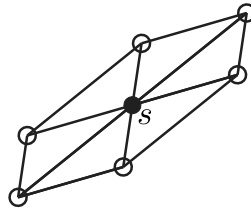
$$f(\Delta_j) = \frac{A_j}{3} (d_H^2(\mathbf{m}_1, \mathbf{x}_i) + d_H^2(\mathbf{m}_2, \mathbf{x}_i) + d_H^2(\mathbf{m}_3, \mathbf{x}_i)) \tag{4}$$

where A_j is the area of Δ_j and $\mathbf{m}_i, i = 1, 2, 3$, are the mid-points on the sides of Δ_j . The gradient $\nabla F_H(\mathbf{X})$ is then computed approximately based on the expression of $f(\Delta_j)$ in Eq. (4).

4.3. Escaping from a poor local minimum

The optimization of the CVT energy function with the HM metric may be trapped at a poor local minimum which results in an undesirable CVT, as shown by the following theorem.

Definition 1 (*Centrosymmetric seed*). A seed s is called a centrosymmetric seed (CS) if its neighbouring seeds (i.e., those seeds sharing at least one Voronoi edge with s) in the Voronoi diagram is centrosymmetric with respect to s . The figure below illustrates a CS s and its six neighbouring seeds in the dual triangulation.



Theorem 2. Given a set of seeds \mathbf{Y} , if \mathbf{Y} consists of only centrosymmetric seeds, the partial derivative of $F_H(\mathbf{Y})$ with respect to each seed in \mathbf{Y} is zero.

The proof of the theorem is given in Appendix B.

Theorem 2 means that when a region R consists solely of CS, the gradient-based optimization of $F_H(\mathbf{X})$ cannot improve further locally in R due to the zero gradient. However, the CS seeds may be arranged in such a way that the dual triangulation of the CVT contains solely of obtuse triangles (as is shown in the triangulation in Fig. 3(a)). We also observe that obtuse triangles often scatter over the domain after an HM CVT optimization, which renders it hard to further decrease the number of obtuse triangles due to the difficulty in fixing an isolated obtuse triangle in an optimization manner. Therefore, we devise a refinement step (Step 3 of the main algorithm) in order to keep the optimization from being trapped at such poor local minima. We note that the isotropic CVT energy function in a convex two-dimensional domain with C^2 density is proved to be C^2 smooth in Liu et al. (2009). Elliptic CVT energy function with a unique elliptic metric inherits the C^2 smoothness and in this case the L-BFGS method converges faster. Also, elliptic CVT is shown to have the ability to cluster nearby obtuse triangles together by our experiments. Therefore, we use the elliptic CVT in an interleaved manner to cluster scattered obtuse triangles together to form connected regions of them. The positions of those seeds incident to an obtuse triangle are then randomly perturbed by at most 0.3 times the average length of their incident edges. Next, an HM CVT optimization is run again to obtain an enhanced result. Multiple passes of this refinement step can be performed if necessary. In this regard, our framework, apart from using a randomly distributed set of points on Ω as the initial seeds, may also accept a partial or complete remeshing result, such as that of an elliptic CVT of Ω as the input.

5. Validation

In this section, we present some experimental results to demonstrate the effectiveness of our method in suppressing obtuse triangles as well as maintaining the anisotropy of a triangulation. All tests are conducted on a PC with a 3.16 GHz Xeon CPU with 8 GB RAM. Also, we use $k = 10$ for our main algorithm which is given in Section 4.

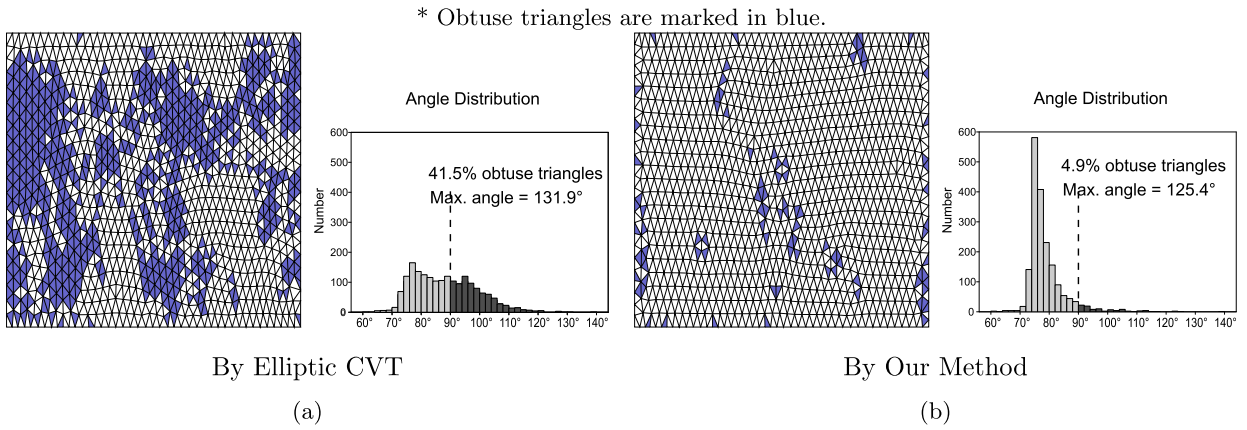


Fig. 5. Triangulation computed by (a) the elliptic CVT method; (b) our method, of 1000 vertices in a square with uniform anisotropy 1 : 2.

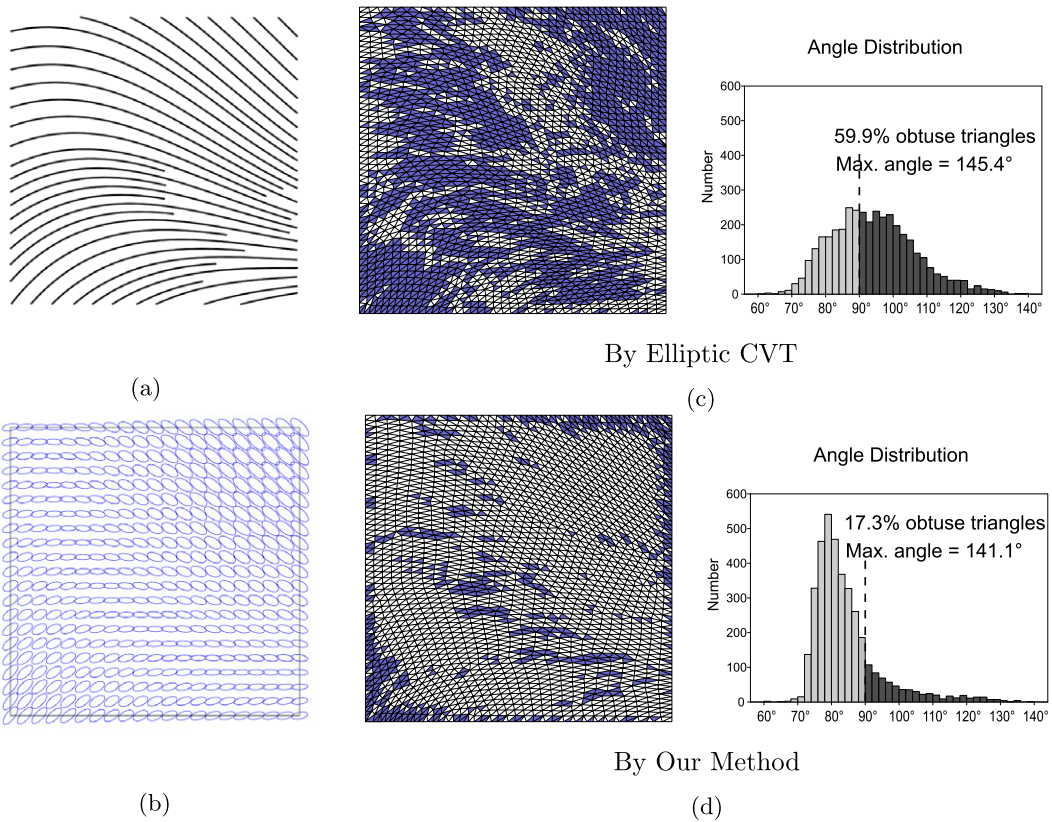


Fig. 6. Triangulations of 2000 points on a two-dimensional domain with varying anisotropy. (a) The input vector field. (b) An elliptic metric tensor is defined based on the vector field. (c) The elliptic CVT generates an anisotropic mesh with 59.9% obtuse triangles. (d) Our method generates an anisotropic mesh of the same anisotropy with 17.3% obtuse triangles. The meshes in (c) and (d) follow the same anisotropy defined in (b).

Fig. 5(a) shows the triangulation of 1000 seeds in a square computed with elliptic CVT, that is, by minimizing $F_E(\mathbf{X})$ in Eq. (2). The mesh has a uniform anisotropy of aspect ratio of 1 : 2, and 41.5% of the triangles are obtuse (marked in blue). In comparison, the triangulation computed with our method has only 4.9% of its triangles being obtuse. Note that, due to boundary effects and difficulty in reaching a global minimum, the obtuse triangles in general cannot be removed completely. The input square domain in this example is a mesh of 19,044 triangles. The computation takes 69 s.

Next, we aim to produce a triangulation of a two-dimensional domain associated with a vector field indicating the desired triangle alignments and elongations (Fig. 6(a)). An anisotropic metric tensor is defined based on the vector field as shown in Fig. 6(b). The input domain is discretized as a mesh of 56,644 triangles and 1000 seeds are used. The elliptic CVT

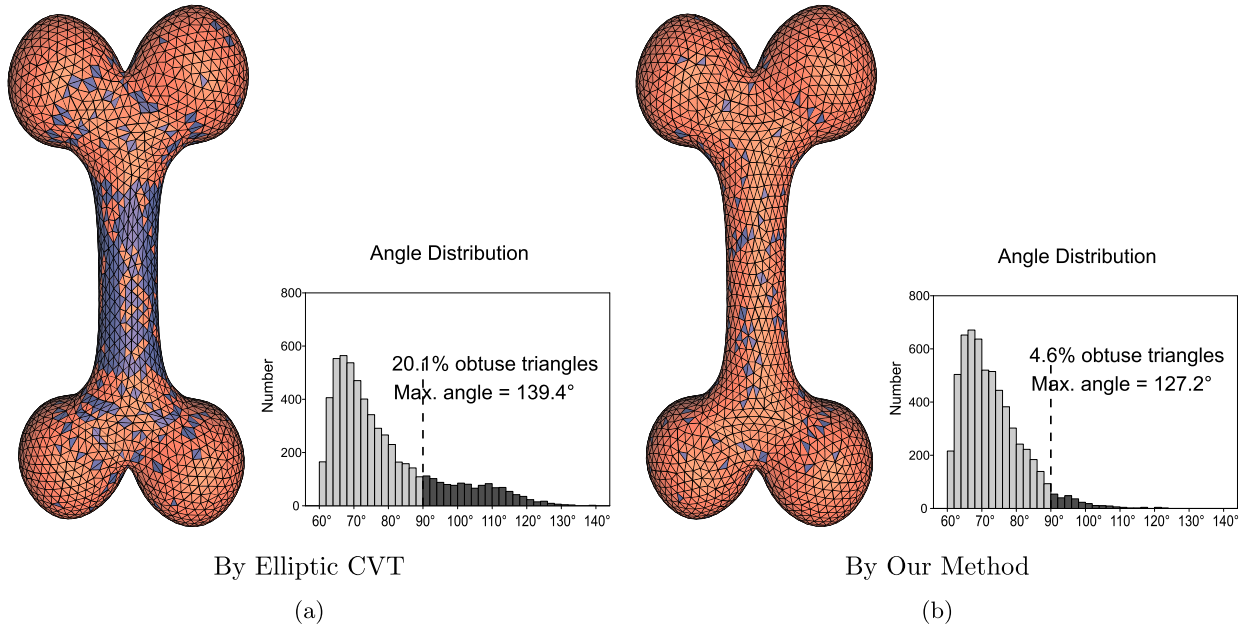


Fig. 7. Anisotropic meshes of 3000 vertices on a bone model. (a) The elliptic CVT generates a mesh with 20.1% obtuse triangles. (b) Our method generates a mesh with 4.6% obtuse triangles, using the result in (a) as the initial input.

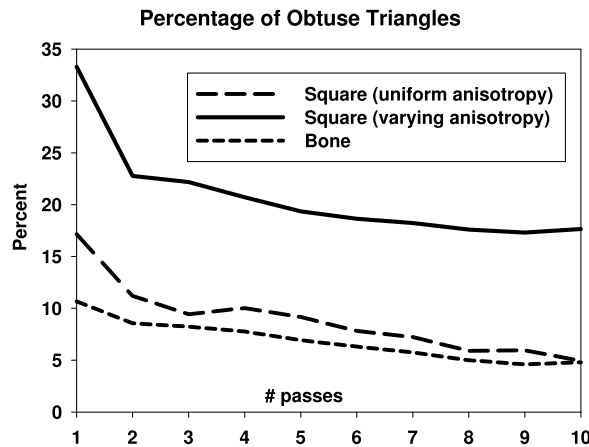


Fig. 8. The number of obtuse triangles after each pass of refinement step for the three examples given in Figs. 5–7. There are a total of $k = 10$ passes.

produces a mesh with 59.9% obtuse triangles (Fig. 6(c)), which is greatly reduced to 17.3% by our method (Fig. 6(d)). Our method takes 261 seconds for generating the triangulation.

Fig. 7 shows another example in which an anisotropic triangulation is generated for a bone-like freeform surface. The anisotropy metric M is defined to depend on the principal curvature directions and the principal curvature magnitudes on the surface. The ratio of the two eigenvalues of the metric M is the largest (about 5 : 1) in the middle part of the bone. The input mesh is of 47,936 triangles and a total of 3000 seeds is used. The elliptic CVT results in 20.1% obtuse triangles which are mainly found on the bone shaft (Fig. 7(a)). Our method based on the HM CVT produces a triangle mesh with 4.6% obtuse triangles (Fig. 7(b)). The total time taken by our method is 244 seconds.

As we have mentioned in Section 4, the refinement procedure, that is, Step 3 of our main algorithm, helps further reduce the number of obtuse triangles. The percentage of obtuse triangles after each pass of the refinement step for all the above three examples are shown in Fig. 8. Generally speaking, the number of obtuse triangles decreases with respect to the number of passes. However, since our framework is variational, the number of obtuse triangle is not strictly decreasing. Nevertheless, after 10 passes of the refinement steps, the number of obtuse triangles can further be reduced by 5% to 15% in the three examples.

We also evaluate how well our resulting triangulation can maintain the anisotropy of a given domain. To evaluate the anisotropy quality of a triangle T at a point \mathbf{p} , we transform T by \mathbf{G}^{-1} to obtain T' , where $\mathbf{G}^T \mathbf{G} = \mathbf{M}^{-1}(\mathbf{p})$ and $\mathbf{M}(\mathbf{p})$

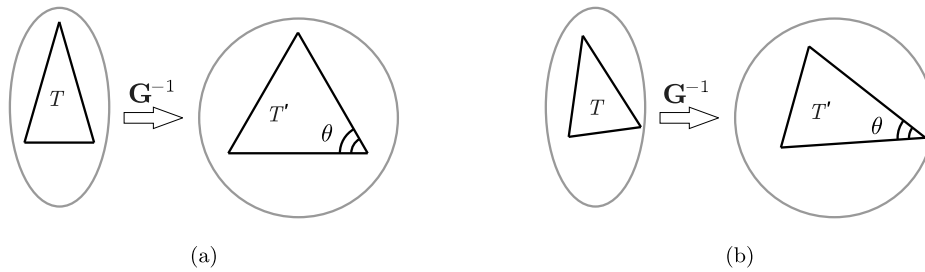


Fig. 9. The affine transformation \mathbf{G}^{-1} transforms the metric tensor ellipse to a circle. (a) A triangle, T , adapting the metric anisotropy well, is transformed to a regular triangle T' . (b) For a triangle T which does not maintain the anisotropy of the metric tensor, the same affine transformation \mathbf{G}^{-1} maps T to a nonregular triangle. The minimal angle θ of the transformed triangle T' thereby provides an anisotropy measure of T .

Table 1

The running time of our algorithm and the anisotropy quality measure of the output triangulations of the three examples given in Figs. 5–7. The qualitative measures for the elliptic CVT method are also provided for comparison. Both the elliptic CVT and our methods capture the anisotropy well. Our method can suppress obtuse triangles effectively while not compromising the anisotropy quality of the triangulations.

	Our method				Elliptic CVT		
	Time (seconds)	Anisotropy quality		# obtuse triangles	Anisotropy quality		# obtuse triangles
		θ_{\min}	θ_{avg}		θ_{\min}	θ_{avg}	
Square (uniform anisotropy)	69	27.1°	53.6°	4.9%	25.2°	52.4°	41.5%
Square (varying anisotropy)	261	20.2°	53.4°	17.3%	8.6°	52.0°	59.9%
Bone	244	27.7°	50.6°	4.6%	21.4°	49.4°	20.1%

is the metric at \mathbf{p} . See Fig. 9 for an illustration. Since \mathbf{G}^{-1} transforms the metric ellipse to a circle which is isotropic, a triangle T that adapts to the anisotropy of the metric ellipse well will be mapped to a triangle T' that is close to a regular triangle. Otherwise, if T does not maintain the anisotropy of the metric ellipse, T' will deviate much from a regular triangle. Hence, we use a common isotropy quality measure of the triangle T' , the minimal angle (denoted by θ) of T' (Frey and Borouchaki, 1997), as the measure of the anisotropy quality of T . It is clear that θ is at most 60 degrees, and the closer θ is to this maximal value, the better the anisotropy quality of T . Of all minimal angles in the transformed triangles (i.e., in the isotropic space), we denote the smallest one as θ_{\min} and their average as θ_{avg} , and use these two values as a measure of the anisotropy quality of a triangulation. The anisotropy quality of the results generated by our method in the above three examples is also shown in Table 1. We note that the anisotropy quality is good, with an average minimal angle of around 50 degrees and a worst case minimal angle of about 20 degrees, which happens in the case of a 2D domain with varying anisotropy. The bone surface example manifests a superior worst case performance with the smallest minimal angle being 27.7 degrees. By comparing with the anisotropy quality of the triangulations generated by the elliptic CVT method, it can be seen that our method can effectively suppress obtuse triangles while not compromising the anisotropy quality of the triangulations.

6. Conclusions

Our method can greatly reduce the number of obtuse triangles in anisotropic meshes, as compared with the conventional CVT-based method. However, because our method is an optimization method, it does not have the ability to reduce the maximal angle of the triangles. Besides that, it still cannot remove obtuse triangles completely. There are at least two reasons for this. The first is due to the boundary effect, that is, obtuse triangles tend to persist along domain boundaries, as shown in the examples in Figs. 5 and 6. The second reason is the difficulty in reaching the global minimizer of the HM CVT energy function, despite our careful optimization strategy that has kept us from getting trapped in poor local minima. Hence, further research is needed to improve the result of the optimization.

Another issue is efficiency. Our current implementation needs several minutes to compute a mesh of moderate size (of several thousand vertices). While slow convergence in CVT computation is certainly a factor, we note that in each iteration, most of the time is spent on computing the anisotropic Voronoi diagram on a mesh. It is envisioned that considerable speedup might be achieved by using surface parametrization with multi-charts and GPU acceleration for computing anisotropic Voronoi diagrams.

Acknowledgements

We thank the reviewers for constructive comments. This work is funded in part by the Research Grant Council of Hong Kong (718010 and 718209), the State Key Program of NSFC project of China (60933008) and the European Research Council (GOODSHAPE ERC-2tG-205693).

Appendix A. Correspondence between an ACVT of a two-dimensional manifold and a CVT of a higher-dimensional Euclidean space

Here we will discuss how the shape of a Voronoi cell of an optimal anisotropic CVT (or ACVT) is determined by a Riemannian metric M . First we will establish the correspondence between an ACVT on a two-dimensional Riemannian manifold Ω and an isotropic CVT in a higher-dimensional Euclidean space. According to Nash’s embedding theorem (Nash, 1956), the surface Ω , as a two-dimensional Riemannian manifold, can be embedded isometrically as a two-dimensional manifold $\hat{\Omega}$ in a Euclidean space \mathbb{E}^k , which is not necessarily three-dimensional—that is, $\hat{\Omega} \subset \mathbb{E}^k$ is equipped with Euclidean metric. Denote this mapping (or embedding) by $R(\mathbf{x}) = \hat{\mathbf{x}} : \Omega \rightarrow \hat{\Omega}$. Clearly, R maps the original anisotropic CVT function $F(\mathbf{X})$ in Eq. (2) to

$$\hat{F}(\hat{X}) = \sum_{i=1}^n \int_{\hat{\Omega}_i} d_E^2(\hat{\mathbf{x}}, \hat{\mathbf{x}}_i) d\sigma,$$

which is the conventional CVT function on $\hat{\Omega}$ with Euclidean metric. It follows that $\hat{F}_i(\hat{X}) \equiv F_i(X)$ for all i and $\hat{F}(\hat{X}) \equiv F(X)$. Hence, the minimization of $F(\mathbf{X})$ is equivalent to that of $\hat{F}(\hat{\mathbf{X}})$ under R .

As proved in Gruber (2001), the Voronoi cell $\hat{\Omega}_i$ of the CVT on the two-dimensional manifold $\hat{\Omega}$ with Euclidean metric is asymptotically a regular hexagon \hat{H} . Let H and \hat{H} be corresponding optimal CVTs on Ω and $\hat{\Omega}$. Consider the corresponding seeds \mathbf{x}_i of H and $\hat{\mathbf{x}}_i$ of \hat{H} . Between the tangent spaces \mathcal{T}_i of Ω at \mathbf{x}_i and $\hat{\mathcal{T}}_i$ of $\hat{\Omega}$ at $\hat{\mathbf{x}}_i$, the metric $\mathbf{M}(\mathbf{x}_i) = (\mathbf{G}^{-1})^T \mathbf{G}^{-1}$ at \mathbf{x}_i induces a linear mapping $\mathbf{v} = \mathbf{G}\hat{\mathbf{v}} : \hat{\mathcal{T}}_i \rightarrow \mathcal{T}_i$, which is the linearization of the stretching of the embedding $R(\mathbf{x})$ of Ω as $\hat{\Omega}$. The linear mapping \mathbf{G}^{-1} maps the regular hexagonal Voronoi cell \hat{H} of the CVT at $\hat{\mathbf{x}}_i$ to an affinely scaled (anisotropic) hexagonal cell H of the ACVT at \mathbf{x}_i , which is inscribed in the ellipse $\mathbf{v}^T M \mathbf{v} = c$ in the tangent plane \mathcal{T}_i , for some constant $c > 0$. Thus, we have determined asymptotically the shape the Voronoi cells of a CVT produced by the anisotropic CVT energy function $F(\mathbf{X})$ in Eq. (2). Furthermore, because $\hat{F}_i(\hat{X}) \equiv F_i(X)$ for all i , it follows from the isotropic case that the anisotropic CVT energy terms $F_i(\mathbf{X})$ are equal for all i asymptotically in an optimal anisotropic CVT.

Appendix B. Proof of Theorem 2

We assume the Riemannian metric defined on the domain Ω is the same everywhere.

Definition 1 (Centrosymmetric seed). A seed s is called a centrosymmetric seed (CS) if its neighbouring seeds (i.e., those seeds sharing at least one Voronoi edge with s) in the Voronoi diagram is centrosymmetric with respect to s .

Definition 2 (Centrosymmetric Voronoi cell). A Voronoi cell is called a centrosymmetric Voronoi cell (CVC) if it is centrosymmetric with respect to the seed of the cell.

Definition 3 (Centrosymmetric pattern). Given a set of seeds \mathbf{Y} , if each Voronoi cell of \mathbf{Y} is a CVC, then \mathbf{Y} form a centrosymmetric pattern (CP).

Lemma 1. *If a seed is a CS, its Voronoi cell is a CVC.*

The proof is simple and is omitted here.

Theorem 2. *Given a set of seeds \mathbf{Y} , if \mathbf{Y} consists of only centrosymmetric seeds, the partial derivative of $F_H(\mathbf{Y})$ with respect to each seed in \mathbf{Y} is zero.*

Proof. Since each seed in \mathbf{Y} is a CS, its Voronoi cell is a CVC. A simple calculation shows that the partial derivative with respect to such a seed is zero. □

References

Babuska, I., Aziz, A.K., 1976. On the angle condition in the finite element method. *SIAM Journal on Numerical Analysis* 13 (2), 214–226.
 Baker, Brenda, Grosse, Eric, Rafferty, Conor, 1988. Nonobtuse triangulation of polygons. *Discrete and Computational Geometry* 3 (1), 147–168.

- Bern, Marshall Wayne, Eppstein, David, 1992a. Mesh generation and optimal triangulation. In: Du, Ding-Zhu, Hwang, Frank Kwang-Ming (Eds.), *Computing in Euclidean Geometry*. In: Lecture Notes Series on Computing, vol. 1. World Scientific, pp. 23–90.
- Bern, Marshall Wayne, Eppstein, David, 1992b. Polynomial-size non-obtuse triangulation of polygons. *International Journal of Computational Geometry & Applications* 2 (3), 241–255. Special issue for 7th SCG.
- Boissonnat, J.-D., Wormser, C., Yvinec, M., 2008. Locally uniform anisotropic meshing. In: *Symposium on Computational Geometry (SOCCG)*, pp. 270–277.
- Bossen, Frank J., Heckbert, Paul S., 1996. A pliant method for anisotropic mesh generation. In: *Proceedings of the 5th International Meshing Roundtable*, pp. 173–190.
- Brandts, J., Korotov, S., Krizek, M., Solc, J., 2009. On nonobtuse simplicial partitions. *SIAM Review* 51, 317–335, doi:10.1137/060669073.
- Cheng, Siu-Wing, Dey, Tamal K., Ramos, Edgar A., Wenger, Rephael, 2006. Anisotropic surface meshing. In: *Proceedings of the Seventeenth Annual ACM-SIAM Symposium on Discrete Algorithms, SODA 2006*, pp. 202–211.
- Cohen-Steiner, David, Alliez, Pierre, Desbrun, Mathieu, 2004. Variational shape approximation. *ACM Transactions on Graphics (Proceeding of SIGGRAPH 2004)* 23 (3), 905–914.
- Dey, Tamal, Levine, Joshua, Wenger, Rephael, 2007. A Delaunay simplification algorithm for vector fields. In: *PG'07: Proceedings of the 15th Pacific Conference on Computer Graphics and Applications*, pp. 281–290.
- Du, Qiang, Wang, Desheng, 2005. Anisotropic centroidal Voronoi tessellations and their applications. *SIAM Journal on Scientific Computing* 26 (3), 737–761.
- Du, Qiang, Faber, Vance, Gunzburger, Max, 1999. Centroidal Voronoi tessellations: Applications and algorithms. *SIAM Review* 41, 637–676.
- Du, Q., Huang, Z., Wang, D., 2005. Mesh and solver co-adaptation in finite element methods for anisotropic problems. *Numerical Methods for Partial Differential Equations* 21, 859–874.
- Dyn, N., Levin, David, Rippa, S., 1990. Data dependent triangulations for piecewise linear interpolation. *IMA Journal of Numerical Analysis* 10 (1), 137–154.
- Dyn, Nira, Hormann, Kai, Kim, Sun-Jeong, Levin, David, 2001. Optimizing 3D triangulations using discrete curvature analysis. In: *Mathematical Methods for Curves and Surfaces: Oslo 2000*. ISBN 0-8265-1378-6. Vanderbilt University, Nashville, TN, USA, pp. 135–146.
- Frey, P., Borouchaki, H., 1997. Surface mesh evaluation. In: *Proceedings of the 6th International Meshing Roundtable*, pp. 363–374.
- Gersho, A., 1979. Asymptotically optimal block quantization. *IEEE Transactions on Information Theory* 25 (4), 373–380.
- Gruber, Peter M., 1999. A short analytic proof of Fejes Tóth's theorem on sums of moments. *Aequationes Mathematicae* 58, 291–295.
- Gruber, Peter M., 2001. Optimal configurations of finite sets in Riemannian 2-manifolds. *Geometriae Dedicata* 84, 271–320.
- Hillion, Pierre, 1977. Numerical integration on a triangle. *International Journal for Numerical Methods in Engineering* 11, 797–815.
- Jiao, Xiangmin, Colombi, Andrew, Ni, Xinlai, Hart, John C., 2006. Anisotropic mesh adaptation for evolving triangulated surfaces. In: *Proceedings of the 15th International Meshing Roundtable*, pp. 173–190.
- Labelle, Francois, Shewchuk, Jonathan Richard, 2003. Anisotropic Voronoi diagrams and guaranteed-quality anisotropic mesh generation. In: *Proceedings of the Nineteenth Annual Symposium on Computational Geometry (SCG'03)*, pp. 191–200.
- Leibon, Greg, Letscher, David, 2000. Delaunay triangulations and Voronoi diagrams for Riemannian manifolds. In: *SCG'00: Proceedings of the Sixteenth Annual Symposium on Computational Geometry*, pp. 341–349.
- Li, J.Y.S., Zhang, H., 2006. Nonobtuse remeshing and mesh decimation. In: *Symposium on Geometry Processing*, pp. 235–238.
- Liu, D.C., Nocedal, J., 1989. On the limited memory BFGS method for large scale optimization. *Mathematical Programming: Series A and B* 45 (3), 503–528.
- Liu, Yang, Wang, Wenping, Lévy, Bruno, Sun, Feng, Yan, Dong-Ming, Lu, Lin, Yang, Chenglei, 2009. On centroidal Voronoi tessellation—energy smoothness and fast computation. *ACM Transactions on Graphics* 28 (4), 1–17.
- Nash, John, 1956. The imbedding problem for Riemannian manifolds. *The Annals of Mathematics* 63 (1), 20–63.
- Rippa, Shmuel, 1992. Long and thin triangles can be good for linear interpolation. *SIAM Journal on Numerical Analysis* 29 (1), 257–270.
- Shewchuk, Jonathan Richard, 2002. What is a good linear element? Interpolation, conditioning, and quality measures. In: *Proceedings of the 11th International Meshing Roundtable*, pp. 115–126.
- Shimada, Kenji, 1997. Anisotropic triangular meshing of parametric surfaces via close packing of ellipsoidal bubbles. In: *Proceedings of the 6th International Meshing Roundtable*, pp. 379–390.
- Simpson, R., 1994. Anisotropic mesh transformations and optimal error control. *Applied Numerical Mathematics* 14 (1–3), 183–198.
- Sun, Feng, Choi, Yi-King, Wang, Wenping, Yan, Dong-Ming, Liu, Yang, Lévy, Bruno, 2010. Obtuse triangle suppression in anisotropic meshes. Technical Report TR-2010-08, Department of Computer Science, University of Hong Kong.
- Valentine, Frederick A., 1964. *Convex Sets*. McGraw-Hill, New York.
- Valette, Sébastien, Chassery, Jean-Marc, Prost, Rémy, 2008. Generic remeshing of 3D triangular meshes with metric-dependent discrete Voronoi diagrams. *IEEE Transactions on Visualization and Computer Graphics* 14 (2), 369–381.
- Wang, Desheng, Du, Qiang, 2005. Mesh optimization based on the centroidal Voronoi tessellation. *International Journal of Numerical Analysis and Modeling* 2, 100–113.